Hindawi
Journal of Engineering
Volume 2022, Article ID 5321046, 19 pages
https://doi.org/10.1155/2022/5321046

Research Article

Performance Analysis and Optimization of Built-In Permanent Magnet and Salient-Pole Electromagnetic Hybrid Excitation Generators for Vehicles

Huihui Geng,[1] Xue-Yi Zhang,[1] Yanhong Gao,[2] Shilong Yan,[1] Yufeng Zhang,[1] Yutong Han,[3] Lei Wang,[4] and Sizhan Hua[1]

[1]*School of Transportation and Vehicle Engineering, Shandong University of Technology, Zibo 255049, China*
[2]*Technology Department, Shandong TangJun Ouling Automobile Manufacturing Co., Ltd., Zibo 255185, China*
[3]*Research and Development Center, Shandong Hapuwo Power Technology Co., Ltd, Zibo 255300, China*
[4]*Technology Center, Weifang No. 1 Motor Factory Co., Ltd., Weifang 262127, China*

Correspondence should be addressed to Xue-Yi Zhang; zhangxueyi@sdut.edu.cn

Received 21 February 2022; Revised 23 March 2022; Accepted 5 April 2022; Published 26 April 2022

Academic Editor: Y.A. Khulief

To solve the problems of the low power density of pure electric excitation generator and nonadjustable magnetic field of pure permanent magnet (PM) generator, a salient-pole hybrid excitation generator (HEG) was proposed in this paper. The designed generator realized coexcitation of two magnetic fields by changing the shape of the pole shoes and embedding the combined-pole PM steels. Compared with other HEGs, it had the advantages of high power density, less excitation loss, and small volume. The paper deduced the analytical expressions of the main magnetic field and armature reaction magnetic field of the HEG and analyzed the armature reaction magnetic circuit, the main influencing parameters, and the influence law of each parameter on the generator output performance to complete the parameter matching of the whole machine. The prototype was trial manufactured and tested with the optimized parameters. The results show that the designed HEG has a low voltage regulation rate, good no-load characteristics, and regulation characteristics. It can ensure the regulated output voltage under rated load conditions and meet the application requirement.

1. Introduction

At present, most of the generators used in vehicles are electric excitation generators, which have the advantages of good magnetic regulation ability and a simple voltage control system [1–5]. However, the excitation winding will consume a lot of energy due to the heating in the process of generating the magnetic field, and it will consume more energy under heavy load conditions, which will cause many problems such as high generator temperature, increased excitation loss, and low output performance [6–11]. In contrast, some vehicles use permanent magnet (PM) generators, which have the advantages of simple structure and high power density. However, the PM magnetic field can not be adjusted and the output voltage is difficult to stabilize, which will lead to the problems of a complex control system, small control range, and low control accuracy [12–17]. Compared with the two types of generators, the hybrid excitation generator (HEG) combines electromagnetic excitation and PM excitation, which has become the focus of research and development trends. It not only can solve the problem of low excitation efficiency of electric excitation generator by reasonably distributing the power of electric excitation magnetic field (EEMF) and PM magnetic field but also can adjust the synthetic magnetic field by adjusting the excitation current to solve the problem of the nonadjustable magnetic field of PM generator [18–24]. However, because the HEG has two types of magnetomotive force sources, it has complex magnetic circuit distribution, diverse topology, and complex performance analysis. Therefore, the research on the

topology structure and performance optimization analysis of the HEG has become the focus of current research.

Many scholars have carried out a lot of research on HEG and achieved some results. The HEG is mainly divided into two types: parallel type and series type. Among them, in the parallel HEG, the PM magnetic field and the EEMF are connected in parallel to provide the main magnetic field. For example, [25–27] all studied the HEG with alternating magnetic poles. In this structure, the PM poles and ferromagnetic poles were alternately attached to the rotor, and the excitation winding was tangentially wound in the center of the stator core. The two magnetic fields were synthesized in the main air gap. Reference [28] proposed a parallel hybrid excitation motor with a PM rotor and claw-pole electric excitation rotor. Two rotors are coaxial and parallel, and a magnetic isolation sleeve is arranged between them. The magnetic fields are independent of each other in the rotor part and were synthesized in the main air gap. In contrast, the two magnetic fields of the series HEG are connected in series to provide the main magnetic field. The series HEG are mainly claw-pole type and salient-pole type. Among them, the claw-pole series HEG usually adds the PM steels between the two yokes or between the two claws. In this way, the PM magnetic field and the EEMF share the claw pole and provide the main magnetic flux in series. For example, [29] proposed a claw-pole series HEG. In this structure, the excitation winding was axially wound between the two flanges, and the PM steel was installed between the front and rear claws in a rectangular shape. The PM magnetic field entered the main air gap through the front and rear claws, and the EEMF was needed through the front claw, rear claw, flanges, and yokes. The two magnetic fields used claws to connect in series to form the main magnetic field. The salient-pole series HEG is divided into two types; one is the salient-pole rotor type. In this type of structure, the pole shoe is embedded with PM steel, the salient-pole body is wound with the excitation winding, and the PM magnetic field and EEMF share the salient-pole rotor to provide the main magnetic flux. For example, [28] proposed a salient-pole PM HEG. In this structure, the rotor changed part of the magnetic poles to built-in PM poles, and the PM poles and the salient poles were connected in series to provide the rotor magnetic field. In order to achieve a brushless structure, the team proposed a HEG with tooth harmonic excitation, in which tooth harmonic winding was slotted outside the PM pole [30]. The other is the double salient-pole structure. The salient-pole stator of this structure is mostly composed of stator blocks, the PM steel is set in the middle of the stator blocks, and the PM magnetic field and the EEMF share the stator to provide the main magnetic field. References [31, 32] both proposed the double salient-pole hybrid excitation flux switching motor. The stators of the two structures were composed of "C" shape and "E" shape stator blocks, respectively, the tangential PM steel was set between the stator blocks, and the excitation winding was wound on the salient pole of the stator. The two magnetic fields were connected in series in the stator to jointly provide the main magnetic field. The comparison of topology structure and performance of HEG is shown in Table 1.

By analyzing the topology structure of various HEGs, it can be concluded that the PM magnetic field and EEMF of the parallel HEG are connected in parallel, and their magnetic circuits are usually independent of each other [13, 33, 34]. Therefore, this type can achieve large output power and have a large magnetic field regulation range. But the two magnetic circuits need to occupy more space, and the structure is usually more complex. In contrast, the series HEG does not occupy additional space. It has the advantages of small volume and lightweight [35]. In the series HEG, compared with the claw-pole type, the salient-pole type has the advantages of small magnetic leakage coefficient and light weight, which is more suitable for vehicle power supply systems. However, at present, salient-pole HEG is mainly based on EEMF and supplemented by PM magnetic field, which is not conducive to reducing excitation loss and improving the applicable reliability. Therefore, this paper proposes a built-in PM and salient-pole electromagnetic HEG. Compared with the conventional salient-pole HEG, the generator is mainly based on the PM magnetic field and supplemented by the EEMF, which can effectively reduce the design power of the electric excitation part and solve the problems of large excitation loss and low output efficiency. Moreover, the PM part adopts the combined-pole structure, and multiple PM steels jointly provide the magnetic field. Compared with the single built-in PM structure, it has higher rotor magnetic field strength and higher generator power density. What is more, reasonably setting the position of the combined-pole PM steels can effectively improve the magnetic field distribution, enhance the sinusoidality of the main magnetic field, and improve the generator output quality.

2. The Structure of Built-In PM and Salient-Pole Electromagnetic HEG

To solve the problems of high excitation loss and low output efficiency of pure salient-pole generators, the combined-pole PM steels are installed at the pole shoes of the salient-pole rotor to provide a magnetic field. This structure can effectively improve the utilization rate of the rotor and improve the power density of the whole generator. The designed HEG is a 3-phase 8-pole 36-slot generator with fractional-slot winding. Its structure is shown in Figure 1. The main technical parameters are shown in Table 2.

As shown in Figure 1, the rotor of the HEG contains both the excitation winding and the PM steels. Due to the demand for EEMF being reduced, the turns of the excitation winding are reduced, and the excess area is given to PM steels. Therefore, the rotor increases the height and width of the pole shoe and sets two rectangular PM steels in the shape of "V" and one semicircular annular PM steel. To increase the magnetic circuit area of the PM steels, the connection shape of the pole shoe and the pole body is changed to excessive inclination. Meanwhile, the semicircular magnetic isolation air gaps are set at both ends of the rectangular PM steels to reduce their end magnetic leakage. The main advantages of the designed HEG are as follows:

Table 1: Comparison of topology structure and performance of HEG.

Category	Feature	Name	Topology structure	Advantages	Disadvantages
Parallel HEG	Two magnetic potential sources are on the stator and rotor, respectively	Alternating magnetic pole HEG	PM steels are attached to the rotor, and excitation winding is wound on the stator core.	The alternating magnetic pole structure effectively reduces the amount of PM materials, and the volume is relatively small.	The excitation winding occupies the armature winding space and magnetic field space, and the output power of the generator is reduced.
	Two magnetic potential sources are on two rotors	PM and claw-pole electromagnetic HEG	The PM rotor and the claw-pole electromagnetic rotor are coaxial and parallel, and they share the same stator.	The magnetic field distribution of the two rotors can be adjusted, and HEG can achieve large output power.	The axial length of the double rotor structure increases, the volume of HEG increases, and the weight is relatively large.
Series HEG	Claw-pole series type	Claw-pole series HEG	The excitation winding is wound axially in the claw-pole flange, and the PM steels are installed in the middle of two claws.	PM steels reduce magnetic leakage between claws and do not occupy additional generator volume.	The claw-pole structure has more magnetic leakage, a small power density, and a large weight.
		Doubly salient-pole hybrid excitation flux switching generator	The stator is composed of stator blocks, the PM steels are sandwiched between the stator blocks, and the excitation winding is wound on stator blocks.	Small size, simple rotor structure, and high-speed operation.	The excitation winding occupies the space of armature winding, and the generator has large vibration and noise.
	Salient-pole series type	Salient-pole HEG with the variable magnetic pole	Changing some magnetic poles, canceling the excitation winding, and building in PM steels.	The PM magnetic field does not occupy additional volume and the generator is small.	During the excitation regulation, the EEMF is not equal to the PM magnetic field, which will affect the distribution of the main magnetic field.
		The designed HEG	Changing the structure of salient-pole shoe and building in combined-pole PM steels.	HEG is mainly based on PM magnetic field and has less excitation loss, small volume, and high power density.	The structure of changing pole shoe increases the winding cost of excitation winding.

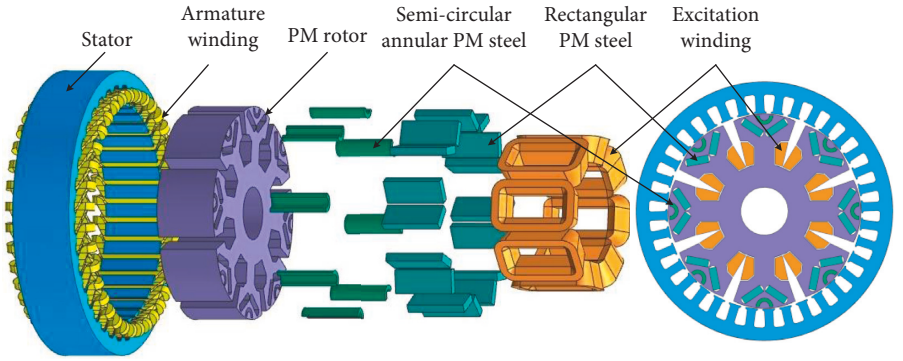

Figure 1: The structure of the designed HEG.

Table 2: Main technical parameters of the designed HEG.

Technical parameter	Parameter value
Rated voltage	28 V
Rated power	1000 W
Rated speed	4000 r/min
Protection grade	IPX 4
Working mode	Continuously working

(a) The PM steel is designed as a combined-pole structure, and the PM magnetic field is jointly provided by multiple PM steels, which makes the generator have a high power density.

(b) The semicircular annular PM steel is set between two V-shaped rectangular PM steels, and its magnetic field direction is basically the same as that of the rectangular PM steels, which makes the PM

magnetic field evenly distributed. Moreover, the design of semicircular annular PM steel can also avoid the problems of the weak central magnetic field of the rotor and high harmonic content of the main magnetic field caused by the magnetic field of V-shaped PM steel concentrated on both sides.

(c) PM steels are set on each rotor pole, and the magnetic field distribution of each pair of magnetic poles is the same. Compared with the rotor structure of partial PM poles, the magnetic field distribution of this design is more uniform, which is conducive to improving the output quality of the generator.

(d) The design of the HEG is mainly based on the PM magnetic field and supplemented by the EEMF. The design power of the PM part is 800 W, while the electric excitation part is 200 W. This design reduces the generator's demand for the EEMF, reduces the excitation loss, and avoids the problem of easy damage to carbon brush and slip ring device under heavy load conditions.

The designed HEG ensures the stability of output voltage by adjusting the magnitude and direction of excitation current. When the load of the generator increases and the output voltage decreases, the generator inputs a large forward excitation current. In this case, the direction of the EEMF is the same as that of the PM magnetic field. The synthetic magnetic field increases, the electromotive force induced by the armature winding increases, and the output voltage increases. When the load of the generator decreases and the output voltage increases, the generator inputs a small forward excitation current. In this case, the direction of the EEMF is the same as that of the PM magnetic field, but the EEMF is weakened, so the synthetic magnetic field is weakened, and the output voltage of the generator is reduced. When the load of the generator is very small and the output voltage of the generator is very large, the generator inputs the reverse excitation current. In this case, the direction of the EEMF is opposite to that of the PM magnetic field. The synthetic magnetic field is the difference between the two magnetic fields. Therefore, when the reverse EEMF increases, the synthetic magnetic field will be significantly weakened, and the output voltage will be reduced to reach the rated output voltage. The magnetic field regulation principle of the designed HEG is shown in Figure 2, and I_f in Figure 2 is the excitation current.

The finite element model of the designed HEG is established and analyzed. When the excitation current is −2 A, 0 A, and 2 A, respectively, the cloud diagram of magnetic flux density is shown in Figure 3.

Figure 3 shows that when the excitation current changes from reverse 2 A to forward 2 A, the magnetic field strength of the generator increases in turn. The effect of the EMMF on the synthetic magnetic field increases from demagnetization to magnetization. The synthetic magnetic field increases, and the output voltage of the generator also increases. When the excitation current is −2 A, 0 A, and 2 A, respectively, the no-load voltage waveform and output voltage variation curve of the generator are shown in Figure 4.

It can be seen from Figure 4 that, with the increase of excitation current, the peak value of the no-load voltage waveform of the generator increases, and the output voltage increases. This shows that adjusting the magnitude and direction of excitation current can realize the regulation of generator output voltage.

3. Analysis of Main Magnetic Field and Armature Reaction Magnetic Field of HEG

When the HEG operates under the load condition, the armature winding will produce armature reaction magnetomotive force, and this magnetomotive force will generate the armature reaction magnetic field. The armature reaction magnetic field will affect the distribution of the main magnetic field and the rotor magnetic field, reduce the output quality of the generator, and even demagnetize the PM steel. Therefore, to accurately analyze the electromagnetic characteristics and output characteristics of HEG, the armature reaction magnetic field and its influence factors on the main magnetic field must be considered. If the influence of the generator end is ignored, the magnetic field model generated by a single conductor in the main air gap is shown in Figure 5.

In Figure 5, *(W)* is the position of the conductor, and point P is any point in the main air gap of the generator, R_0 is the radius of the stator inner circle, and R_1 is the radius of the rotor outer circle. The main air gap of the generator is a 2D parallel plane field [36], which satisfies the Poisson equation:

$$\frac{\partial^2 A_z}{\partial r^2} + \frac{1}{r}\frac{\partial A_z}{\partial r} + \frac{1}{r^2}\frac{\partial^2 A_z}{\partial \theta^2} = -\mu_0 J_z, \tag{1}$$

where A_z is the vector magnetic potential of the main air gap in the Z-axis direction, r is the radius from point P to the rotor center, θ is the angle between the connecting line from point P to the rotor center and the connecting line between the conductor and the rotor center, μ_0 is the vacuum permeability, and J_z is the current density.

The area of the main air gap belongs to the noncurrent-carrying area, and $A_z = 0$, so the modified Poisson equation is as follows:

$$\frac{\partial^2 A_z}{\partial r^2} + \frac{1}{r}\frac{\partial A_z}{\partial r} + \frac{1}{r^2}\frac{\partial^2 A_z}{\partial \theta^2} = 0. \tag{2}$$

Assuming that the reluctance of the generator core is infinite, the boundary conditions are set as

$$\begin{cases} B_\theta|_{r=R_0} = 0, \\ \\ B_\theta|_{r=R_1} = \dfrac{\mu_0 i}{2\pi R_0}, \end{cases} \tag{3}$$

where i is armature winding current.

Define a as the distance between the conductor and the rotor center. When $r \geq a$, the tangential and radial

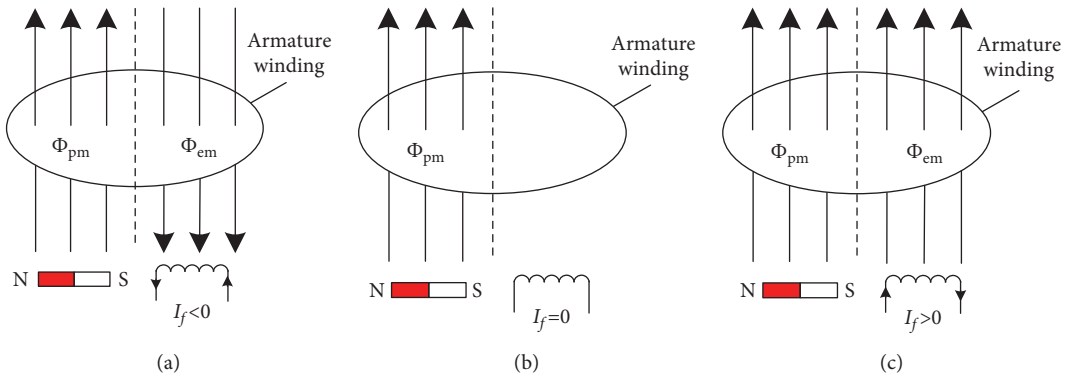

Figure 2: Schematic diagram of magnetic field regulation of HEG: (a) when the excitation current is less than 0 A; (b) when the excitation current is equal to 0 A; (c) when the excitation current is greater than 0 A.

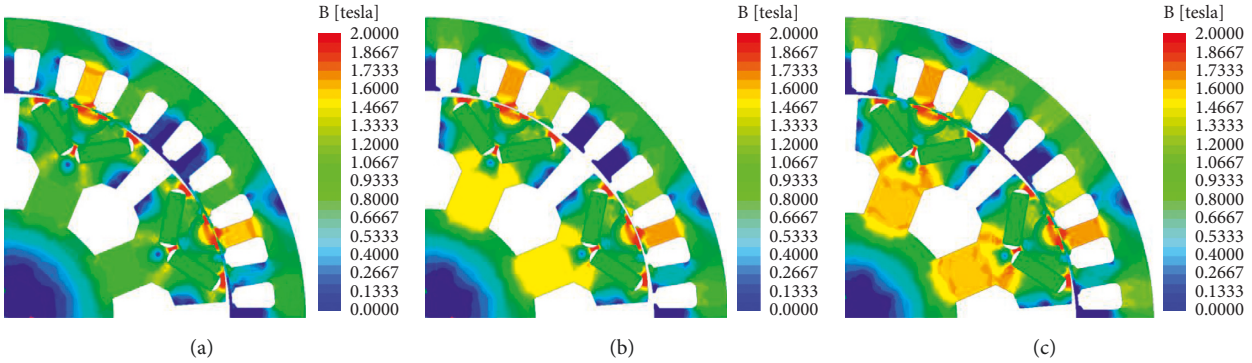

Figure 3: Cloud diagrams of magnetic flux density with different excitation currents: (a) when the excitation current is−2 A; (b) when the excitation current is 0 A; (c) when the excitation current is 2 A.

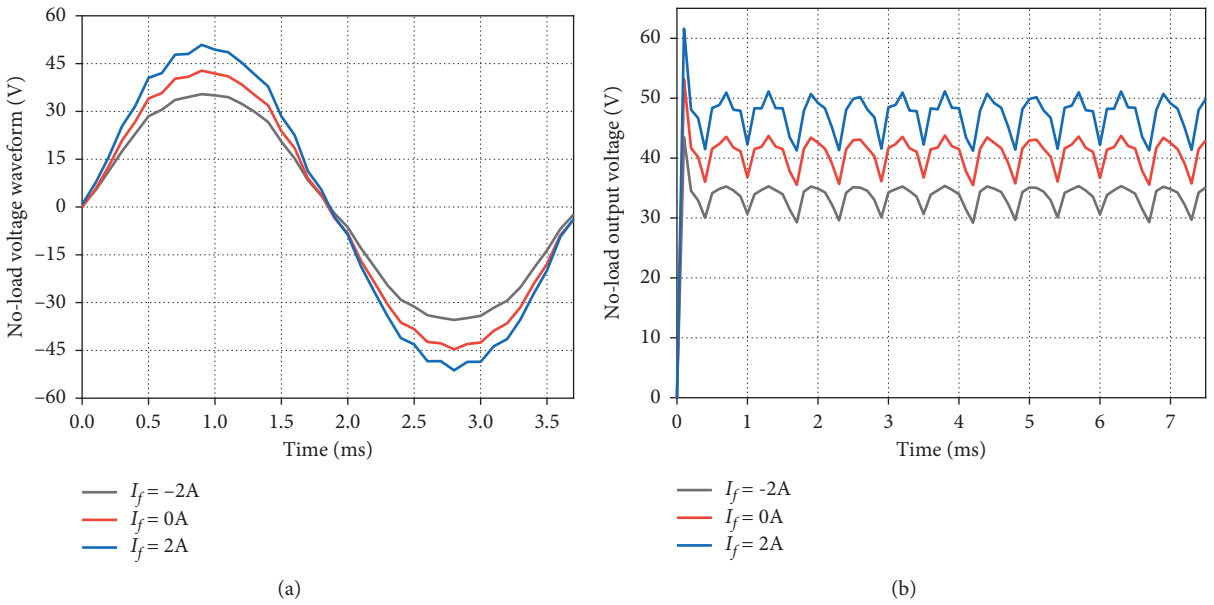

Figure 4: No-load voltage waveform and output voltage variation curve of the generator with different excitation currents: (a) no-load voltage waveform; (b) output voltage variation curve.

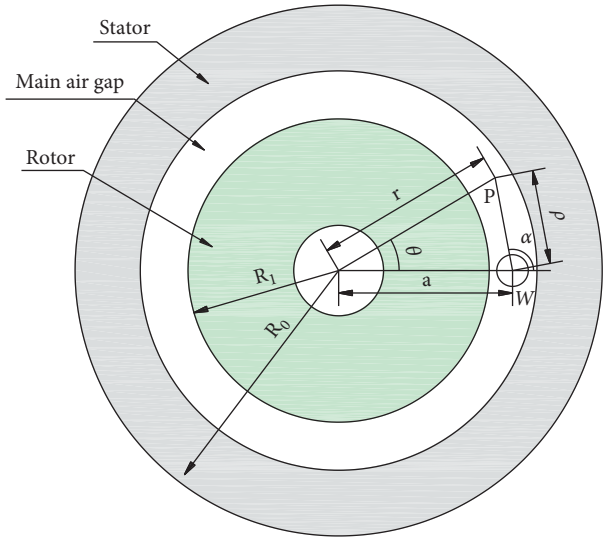

Figure 5: Simplified magnetic field model of single armature winding of HEG.

components of the magnetic flux density in the main air gap can be obtained as

$$\begin{cases} B_\theta = \dfrac{\mu_0 i}{2\pi r}\left[1 + \sum\limits_{m=1}^{\infty} \dfrac{R_0^m}{a^m}\left(\dfrac{a^{2m} + R_1^{2m}}{R_0^{2m} - R_1^{2m}}\right)\left(\dfrac{R_0^m}{r^m} - \dfrac{r^m}{R_0^m}\right)\cos\, m\theta\right], \\ B_r = -\dfrac{\mu_0 i}{2\pi r}\sum\limits_{m=1}^{\infty} \dfrac{R_0^m}{a^m}\left(\dfrac{a^{2m} + R_1^{2m}}{R_0^{2m} - R_1^{2m}}\right)\left(\dfrac{r^m}{R_0^m} + \dfrac{R_0^m}{r^m}\right)\sin\, m\theta, \end{cases} \tag{4}$$

where B_θ is the tangential component of the magnetic flux density, and the B_r is the radial component of the magnetic flux density.

When the conductor is on the stator surface, and $a = R_0$, the above formula is simplified to

$$\begin{cases} B_\theta = \dfrac{\mu_0 i}{2\pi r}\left[1 + \sum\limits_{m=1}^{\infty}\left(\dfrac{R_0^{2m} + R_1^{2m}}{R_0^{2m} - R_1^{2m}}\right)\left(\dfrac{R_0^m}{r^m} - \dfrac{r^m}{R_0^m}\right)\right], \\ B_r = -\dfrac{\mu_0 i}{2\pi r}\sum\limits_{m=1}^{\infty}\left(\dfrac{R_0^{2m} + R_1^{2m}}{R_0^{2m} - R_1^{2m}}\right)\left(\dfrac{r^m}{R_0^m} + \dfrac{R_0^m}{r^m}\right). \end{cases} \tag{5}$$

In the same way, the tangential and radial components of the magnetic flux density in the main air gap generated by the single armature winding can be obtained as

$$\begin{cases} B_\theta = \dfrac{\mu_0 i}{2\pi r}\left[1 + \sum\limits_{m=1}^{\infty}\left(\dfrac{R_0^{2m} + R_1^{2m}}{R_0^{2m} - R_1^{2m}}\right)\left(\dfrac{R_0^m}{r^m} - \dfrac{r^m}{R_0^m}\right)\right]\sin(m\varepsilon)\sin\, m\theta, \\ B_r = \dfrac{\mu_0 i}{2\pi r}\sum\limits_{m=1}^{\infty}\left(\dfrac{R_0^{2m} + R_1^{2m}}{R_0^{2m} - R_1^{2m}}\right)\left(\dfrac{r^m}{R_0^m} + \dfrac{R_0^m}{r^m}\right)\sin(m\varepsilon)\cos\, m\theta. \end{cases} \tag{6}$$

Ignoring the effect of core saturation, the armature winding located in the stator slot is equivalent to the conductor located on the centerline of the slot. The equivalent current is expressed as $I(t) = N_s i(t)$, where N_s is the turns of the armature winding. Based on this, when the A-phase armature winding passes through the current $i(t)$, the radial component of the air-gap magnetic density of the armature reaction magnetic field can be calculated as

$$\begin{aligned} B_{ra}(r,\theta,t) = {} & \sum_{k=1}^{N_s} C_k \frac{\mu_0 I(t)}{2\pi r}\sum_{m=1}^{\infty}\left(\frac{R_0^{2m} + R_1^{2m}}{R_0^{2m} - R_1^{2m}}\right) \\ & \cdot\left(\frac{r^m}{R_0^m} + \frac{R_0^m}{r^m}\right)\sin(m\varepsilon)\cos\left[m\left(\theta + \beta_k\right)\right], \end{aligned} \tag{7}$$

where C_k is the direction of the armature winding current, ε is the armature winding span angle, and β_k is the distance angle between the centerline of armature winding of group k and the centerline of A-phase armature winding.

According to (7), the magnitude of the armature reaction magnetic field is mainly related to the armature winding and armature current. For the generator, the armature current is related to the generator output power and the rated load. After the armature reaction magnetic field is generated, its magnetic circuit is formed by the stator core, main air gap, and rotor core. So, the armature reaction magnetic field is also affected by the main air gap and rotor structure. The magnetic circuit is different due to the different rotor structures, and the change of the main magnetic field caused by it is also different. When the PM rotor has a pole shoe, the armature reaction magnetic flux will be mainly closed through the pole shoe. Moreover, when the height of the pole shoe reaches a certain level, the PM steel is hardly affected by the armature reaction. In this case, the influence of the main magnetic field is the same as that of the electric excitation generator. Meanwhile, the main magnetic field will return to the previous state when the load is removed. However, when the PM rotor has no pole shoe, the armature reaction magnetic flux will be closed through the PM steel. Due to the resistance of the PM steel being large, it will absorb more armature reaction magnetic field. Under high-power conditions, the PM steel may have the problem of demagnetization. In this design, the PM steel is a built-in structure. The rotor core on the outside of the PM steel is equivalent to the pole shoe, which has a certain protective effect on PM steel. When the centerline of the rotor magnetic pole is collinear with the centerline of the A-phase armature winding, the armature reaction magnetic circuits and the main magnetic flux circuits at the center of the rotor magnetic pole are shown in Figure 6.

As shown in Figure 6, the main magnetic flux circuit forms a circuit through two adjacent salient poles, and the armature reaction magnetic circuit mainly passes through the center of the magnetic pole. The armature reaction magnetic field mainly has three magnetic circuits, and the three magnetic circuits all pass through the stator core and reach the rotor pole shoe through the main air gap. In magnetic circuit 1, the armature reaction magnetic flux passes through the pole shoe on the outer side of the semicircular annular PM steel and returns to the main air

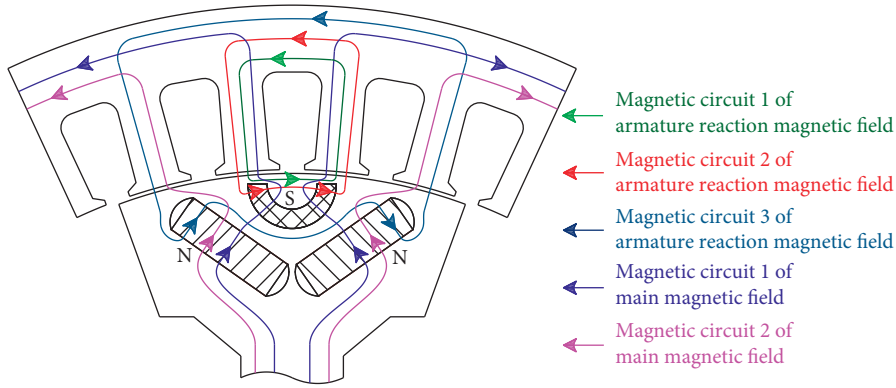

Figure 6: The magnetic circuit of the armature reaction magnetic field.

gap. In magnetic circuit 2, the armature reaction magnetic flux passes through the pole shoe and the left and right ends of the semicircular annular PM steel and then returns to the main air gap. In magnetic circuit 3, the armature reaction magnetic flux passes through the two rectangular PM steels and the pole shoe and then returns to the main air gap. In three magnetic circuits, because magnetic circuit 1 does not pass through the PM steel, its reluctance is small. Magnetic circuit 2 only passes through the semicircular annular PM steel; it has a relatively large reluctance. Magnetic circuit 3 needs to pass through two rectangular PMs; it has the largest reluctance. Therefore, the three magnetic circuits are sorted according to the size of the resistance: magnetic circuit 3 > magnetic circuit 2 > magnetic circuit 1. Based on the principle of minimum reluctance, the armature winding magnetic field is mainly distributed in magnetic circuit 1, followed by magnetic circuit 2 and magnetic circuit 3.

According to the analysis of the armature reaction magnetic circuits, the armature reaction magnetic field is equivalent to the magnetomotive force F_{ac} in series with the armature winding internal resistance R_{ac}, and the equivalent magnetic circuit diagram can be drawn and shown in Figure 7.

In Figure 7, Φ_{d1} is the total magnetic flux generated by the armature reaction magnetomotive force. Φ_{r1}, Φ_{r2}, and Φ_{d3} are the magnetic flux in the rotor of the magnetic circuit 1, magnetic circuit 2, and magnetic circuit 3, respectively. Φ_{d2} is the magnetic flux in the rotor between the magnetic circuit 1 and magnetic circuit 2. R_{se} and R_{sc} are the reluctance of the stator yoke and stator teeth, respectively. R_δ is the reluctance of the main air gap. R_{pc} and R_{pv} are the reluctance of semicircular annular PM steel and rectangular PM steel. R_{r1}, R_{r2}, R_{r3}, R_{r4}, and R_{r5} are the reluctance of the rotor core in the pole shoe of magnetic circuit 1, magnetic circuit 2, and magnetic circuit 3, respectively.

Figure 7 clearly shows the main influencing parameters of the armature reaction magnetic field, and it is convenient for analyzing and optimizing the magnetic circuit distribution. According to the equivalent magnetic circuits, the main influencing factors include armature winding, stator slot, main air gap, and rotor pole shoe. Among them, the internal resistance of armature winding is mainly determined by its turns and its wire diameter. In this design, since

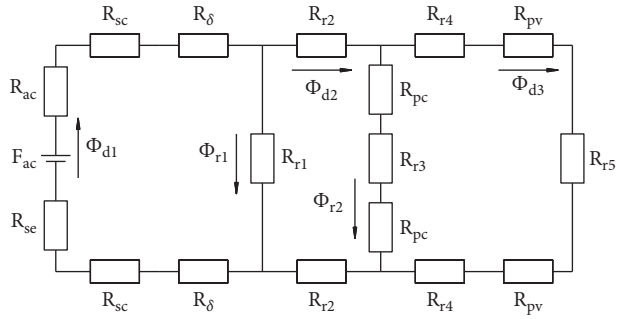

Figure 7: Equivalent magnetic circuit diagram of armature reaction magnetic field.

the wire diameter needs to be standard diameter, two enameled wires with the diameter of 0.67 mm and 0.72 mm are selected for the designed generator, and the wire diameter is not considered.

4. Parameter Analysis of the Designed HEG

The armature reaction magnetic field mainly affects the output voltage under the load condition, which can be analyzed by the voltage regulation rate ΔU. The voltage regulation rate of the HEG is calculated as the value when the excitation current is 0; in other words, the voltage regulation rate of the EEMF is not considered. The calculation formula of the voltage regulation rate is as follows.

$$\Delta U = \frac{U_0 - U_N}{U_N} \times 100\%, \tag{8}$$

where U_0 is the generator output voltage under no-load condition, U_N is the generator output voltage under rated load condition, since the EEMF part is ignored, the rated load condition is defined as the condition where the excitation current is 0 A, and the rated power is 800 W.

The finite element model of the designed generator is established and simulated, and the variation curves of the generator output voltage under rated load condition, voltage regulation rate, and THD (total harmonic distortion) of no-load voltage with the different armature winding turns are obtained and shown in Figure 8.

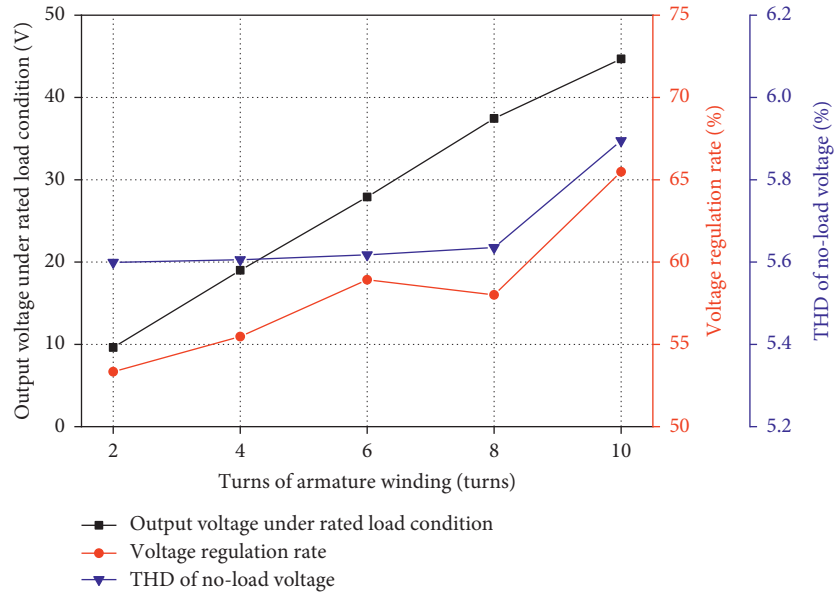

Figure 8: Variation curves of generator output performance with different armature winding turns.

Figure 8 shows that with the increase of the turns of the armature winding, the generator output voltage under rated load conditions increases almost linearly, the voltage regulation rate increases slowly, its upward trend increases when the armature winding turns is 8 turns, and the THD of no-load voltage waveform is basically unchanged at first and rises rapidly when the turns are 8 turns. Meanwhile, with the increase of armature winding turns, the generator output voltage increases, the armature reaction magnetic field increases, and the copper loss will also increase. According to the output voltage under rated load conditions, when the turns of armature winding are greater than 6 turns, the output voltage is greater than 28 V, which meets the design power requirements. Therefore, the turns of armature winding are selected as 6 turns.

The stator slot parameters that affect the armature reaction magnetic field mainly include stator slot width, stator slot height, and stator slot notch width. Among them, when the turns of the armature winding are constant, the stator slot area is basically determined. Therefore, when considering the stator slot parameters, the constant stator slot area is taken as the constraint condition, and only the two variables of stator slot width and stator slot width are considered. The variation curves of generator output performance with different stator slot widths are shown in Figure 9.

Figure 9 shows that with the increase of the stator slot width, the THD of the no-load voltage of the generator increases, and the generator output voltage and the voltage regulation rate both increase first and then decrease. The output voltage reaches the maximum value when the stator slot width is 5.8 mm, and the voltage regulation rate reaches the maximum value when the stator slot width is 5.4 mm. In order to ensure that the area of the stator slot and the turns of armature winding remain unchanged, the smaller the stator slot width, the deeper the stator slot and the lower the height of the stator yoke; this state is easy to cause the magnetic field saturation of the stator yoke. On the contrary, the larger the stator slot width, the smaller the stator tooth width; this state is easy to cause the magnetic field saturation of the stator tooth. Through comprehensive analysis, it is appropriate to select the stator slot width from 5.8 mm to 6.4 mm.

Different stator slot notch widths will cause the change of resistance at the top of the stator tooth, resulting in the change of the main magnetic field and armature reaction magnetic field. Therefore, the influence laws of different stator notch widths on the output performance of the generator are analyzed and shown in Figure 10.

It can be seen from Figure 10 that with the increase of the stator notch width, the generator output voltage under rated load conditions decreases, and the voltage regulation rate and the THD of no-load voltage both increase. In other words, the smaller the stator notch width, the better the generator output performance. However, if the stator notch width is too small, it will make winding difficult and increase the processing cost. Comprehensively, it is appropriate to take the stator notch width from 2.6 mm to 2.8 mm. Since different stator slot widths and different stator notch widths should cooperate with each other, in other words, if the stator slot width is large, the corresponding stator notch width should be increased appropriately, and vice versa. Therefore, when the two parameters change at the same time, the variation diagrams of generator output performance are analyzed and shown in Figure 11.

Figure 11 shows that when the generator is under rated load condition, the combination parameters of small stator notch width and moderate stator slot width can achieve large output voltage, and the smaller stator notch width and larger stator slot width can obtain lower voltage regulation rate and the THD of no-load voltage. However, considering the increase in processing cost caused by a small stator notch, the width of the stator notch is selected as 2.6 mm, and the

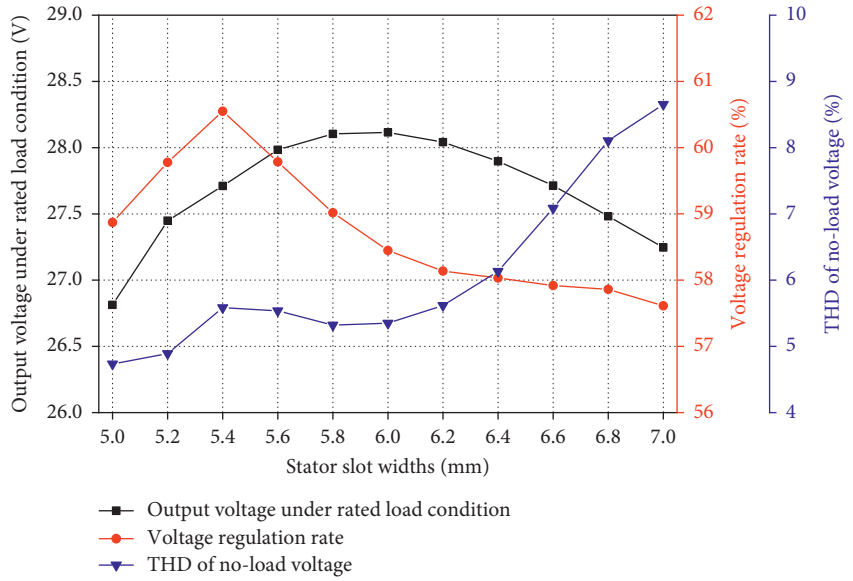

Figure 9: Variation curves of generator output performance with different stator slot widths.

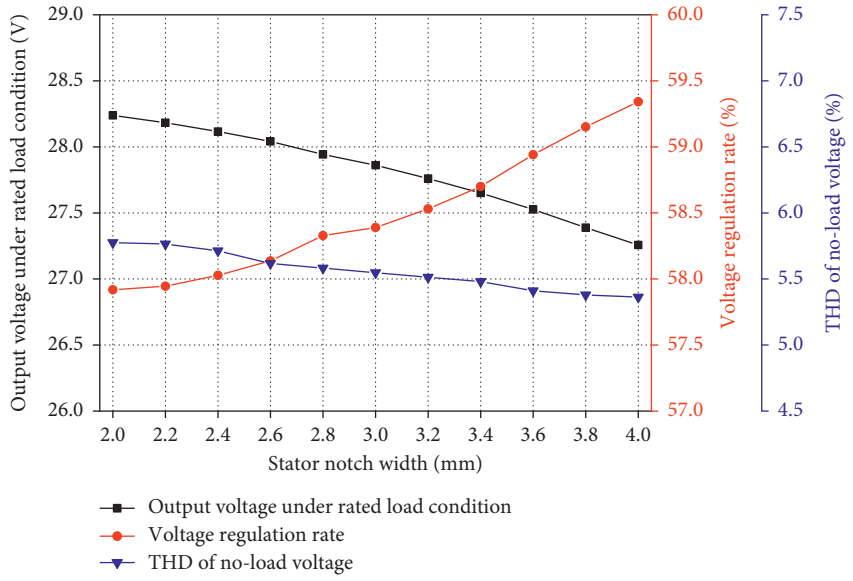

Figure 10: Variation curves of generator output performance with different stator notch widths.

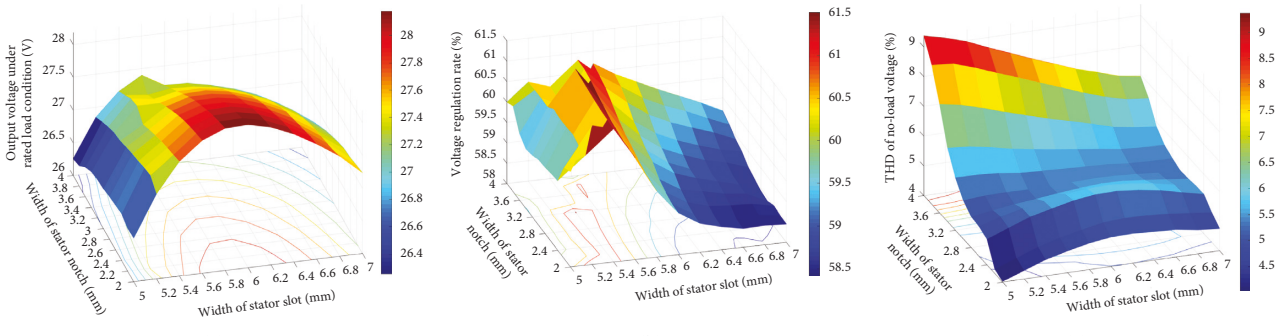

(a) (b) (c)

Figure 11: Variation diagrams of generator output performance with different stator slot widths and different stator notch widths: (a) output voltage under rated load condition; (b) voltage regulation rate; (c) THD of no-load voltage.

width of the stator slot is selected as 6.2 mm. In this case, the generator output voltage under rated load condition is 28.1 V, the voltage regulation rate is 58.2%, and the THD of no-load voltage is 5.6%.

The main air gap of the generator is the position of the main magnetic field and the main reluctance of the armature reaction magnetic field. The greater the main air gap length, the greater its magnetic resistance. Its influence on the main magnetic field and armature reaction magnetic field will be weakened. The influence laws of different lengths of the main air gap on the generator output performance are analyzed, as shown in Figure 12.

It can be seen from Figure 12 that with the increase of the length of the main air gap, the generator output voltage and the THD of no-load voltage gradually decrease, and the voltage regulation rate gradually increases and then tends to remain unchanged. It shows that the smaller the length of the main air gap, the better the output performance of the generator. However, the smaller the main air gap, the higher the processing cost. In this paper, the main air gap of the generator is selected as 0.4 mm.

To obtain a better sinusoidal distribution of the main magnetic field, the nonuniform air gap is often used in vehicle generators. The nonuniform air gap takes the angle of one rotor magnetic pole as the variation range and takes the point on the centerline of the rotor magnetic pole with a certain distance away from the rotor center as the eccentric center, which is recorded as O_1. The rotor outer circle of nonuniform air gap takes O_1 as the center and the distance between O_1 and the outer circle of the original rotor as the radius. The nonuniform air gap is shown in Figure 13.

As shown in Figure 13, the distance between the eccentric center O_1 and the original rotor center O_0 is defined as the rotor eccentricity, which is recorded as h_r. When h_r is from 0 mm to 20 mm, and the step is 2 mm, the variation curves of generator output performance are shown in Figure 14.

Figure 14 shows that with the increase of the rotor eccentricity, the generator output voltage gradually increases, and the voltage regulation rate and the THD of no-load voltage decrease gradually. These show that the larger the rotor eccentricity, the better the output performance of the generator. The reason is that when the rotor eccentricity increases, the outer circle arc of the rotor is bent, the length difference of the main air gap between the center and both sides of the rotor magnetic pole becomes larger, and the nonuniformity of the main air gap increases. This is more conducive to improve the sinusoidality of the main air-gap magnetic field. However, the larger the rotor eccentricity, the closer the rotor outer circle is to the rectangular PM steel, and the strength of the rotor structure decreases. Through comprehensive analysis, it is appropriate to select the rotor eccentricity from 14 mm to 16 mm.

The magnetic circuit 1 in the rotor pole shoe mainly depends on the distance between the outside of the semicircular annular PM steel and the rotor outer circle. This distance is recorded as the outer length of semicircular annular PM steel, which is represented by h_o, as shown in Figure 13. The greater the h_o, the farther the semicircular annular PM steel from the rotor outer circle, and the more armature reaction magnetic flux the magnetic circuit 1 passes through. However, if h_o is too large, the magnetic gathering effect of the semicircular annular PM steel will be very small, and the magnetic circuit distribution of the rectangular PM steel will be affected. Therefore, this distance length should be reasonably analyzed. When h_o takes 0.6 mm to 3.2 mm and the step size is 0.2, the variation curves of the generator output performance are shown in Figure 15.

Figure 15 shows that with the increase of h_o, the generator output voltage decreases rapidly and tends to be stable after h_o is 2.4 mm. The change of THD of no-load voltage is opposite to it. The voltage regulation rate shows a gradual upward trend. When h_o is small, the semicircular annular PM steel is close to the rotor outer circle, and the resistance of the armature reaction magnetic field at the rotor pole increases. In this case, the armature reaction magnetic field is weak, the generator output voltage is high, and the voltage regulation rate is low. The result is the same as the above magnetic circuit analysis result. However, if h_o is too small, the structural strength of semicircular annular PM steel will be reduced. It is appropriate to select h_o from 1 mm to 1.2 mm.

The equivalent magnetic circuit diagram shows that the main influencing factors of magnetic circuit 2 are the parameters of the semicircular annular PM steel and the magnetic circuit of the rotor core. Among them, the reluctance of the semicircular annular PM steel is mainly related to its thickness. The rotor magnetic circuit is mainly related to the inner diameter of the semicircular annular PM steel. Therefore, through the combined parameter analysis of the thickness and inner diameter of semicircular annular PM steel, the variation diagrams of the generator output performance are shown in Figure 16.

It can be seen from Figure 16 that when the generator operates under the rated load condition, the larger inner diameter and the moderate thickness of the semicircular annular PM steel can obtain a larger output voltage, the larger thickness will lead to a higher voltage regulation rate, and the larger inner diameter will lead to a higher THD of no-load voltage. Considering comprehensively, it is appropriate to select the thickness of semicircular annular PM steel from 2 mm to 2.5 mm and select the inner diameter from 2.6 mm to 2.8 mm.

The equivalent magnetic circuit diagram of magnetic circuit 3 shows that the main influencing factors are the parameters of the rectangular PM steel and the parameters of the rotor magnetic circuit. Among them, the reluctance of the rectangular PM steel is mainly related to its width. Therefore, when the width of rectangular PM steel changes, the variation curves of the output performance of the generator are analyzed as shown in Figure 17.

Figure 17 shows that with the increase of the width of rectangular PM steel, the generator output voltage gradually increases and reaches the rated output voltage when the width is greater than 4 mm. The voltage regulation rate gradually decreases and then increases and reaches the minimum value when the width is 3.5 mm. Meanwhile, the

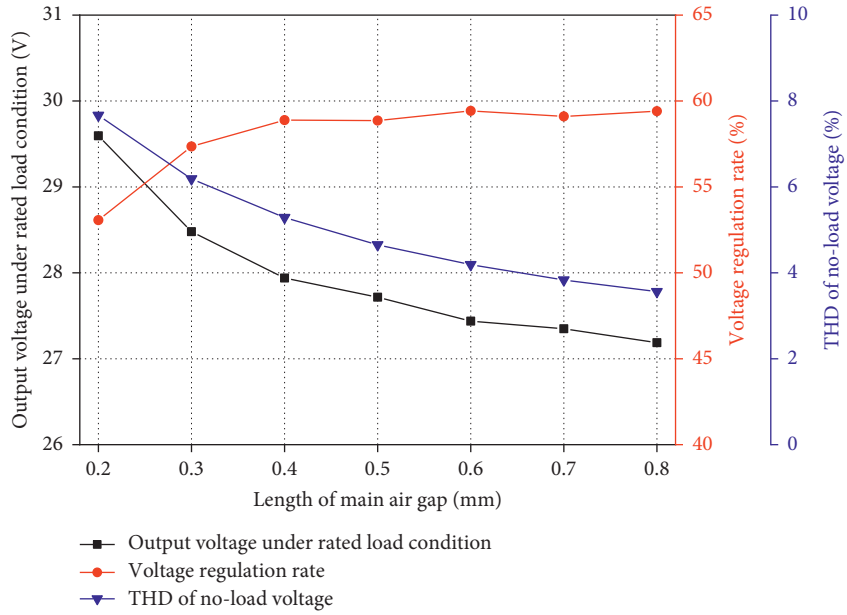

Figure 12: Variation curves of generator output performance with different lengths of the main air gap.

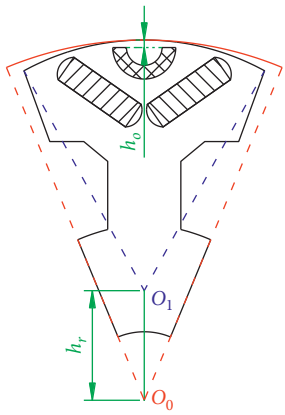

Figure 13: Schematic diagram of the nonuniform air gap.

THD of no-load voltage first decreases and then increases and reaches the minimum value when the width is 4 mm. With the increase of the width, the PM magnetic field provided by it increases, and the generator output voltage under load conditions also increases. But the reluctance of the magnetic circuit 2 increases and the armature reaction magnetic field weakens. Overall, the magnetizing effect of the PM magnetic field counteracts the weakening effect of the armature reaction magnetic field, and the voltage regulation rate of the generator changes little. Moreover, the amount of PM materials will increase with the increase of its width, and it is appropriate to select the width of rectangular PM steel from 3.5 mm to 4.5 mm.

The rotor magnetic circuit of magnetic circuit 3 is mainly related to the width of the rotor pole shoe and the position parameters of two rectangular PM steels. Among them, to reduce the magnetic leakage at the inner ends of the rectangular PM steels and ensure the constant distance between the inner ends, the inclination angle and length of the rectangular PM steel are defined as the research parameters. The smaller its inclination angle and the longer its length, the closer it is to the rotor outer circle. When the length of rectangular PM steel changes from 9 mm to 14 mm with the step length of 0.5 mm, the inclination angle changes from 40 to 60 with the step degree of 2, and the variation curves of the output performance of the generator are analyzed and shown in Figure 18.

Figure 18 shows that when the generator is under the rated load condition, the large rectangular PM steel length and large inclination angle can obtain the large output voltage. With the increase of the length and inclination angle, the generator output voltage increases almost linearly and the voltage regulation rate decreases almost linearly. But the THD of the no-load voltage of the generator decreases first and then increases and reaches the minimum value when the length of rectangular PM steel is 11.5 mm. Therefore, it is appropriate to select the length from 11 mm to 12 mm. When the inclination angle is 55° and the length is 12 mm, the output voltage reaches 28 V under rated load conditions. The inclination angle of rectangular PM steel is selected between 54 and 56.

Different pole-arc coefficients can affect the area of the PM magnetic field in the rotor pole shoe and affect the distribution of the armature reaction magnetic field. Therefore, it is necessary to analyze the output performance of the generator with different pole-arc coefficients, and the results are shown in Figure 19.

Figure 19 shows that with the increase of the pole-arc coefficient, the generator output voltage gradually decreases and then tends to be stable. The voltage regulation rate decreases when the pole-arc coefficient is from 0.76 to 0.82 and remains unchanged at other times. The THD of no-load voltage shows a gradual upward trend as a whole. In other words, the smaller the pole-arc coefficient, the better the output performance of the generator. However, due to the

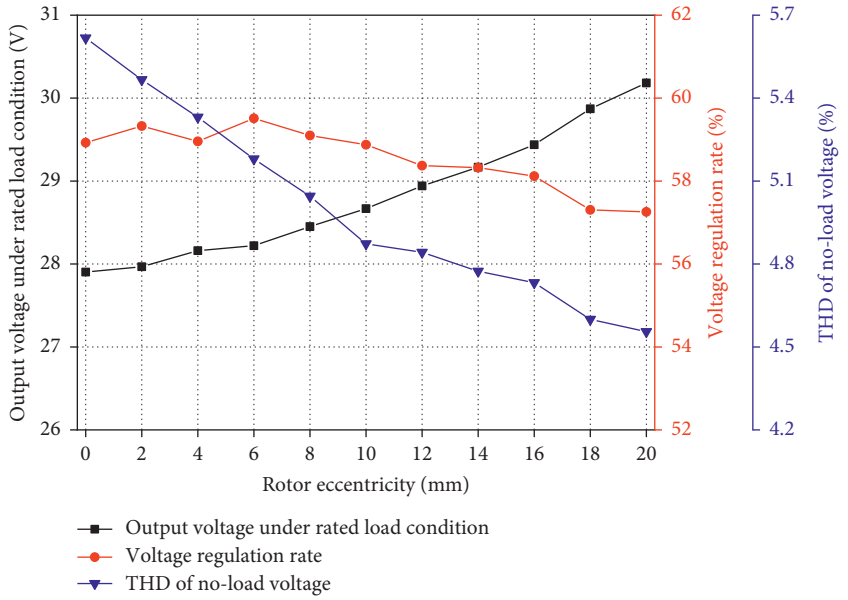

Figure 14: Variation curves of generator output performance with different rotor eccentricities.

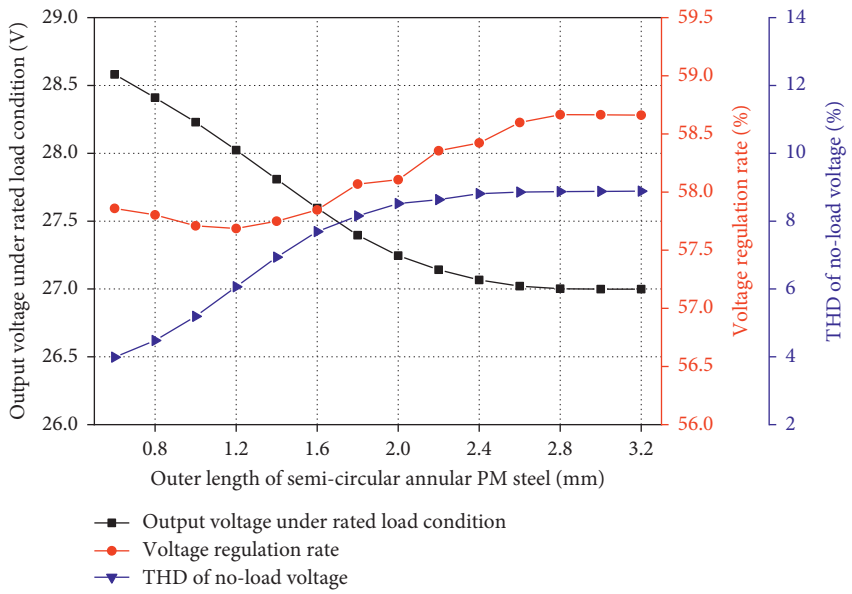

Figure 15: Variation curves of generator output performance with different outer lengths of semicircular annular PM steel.

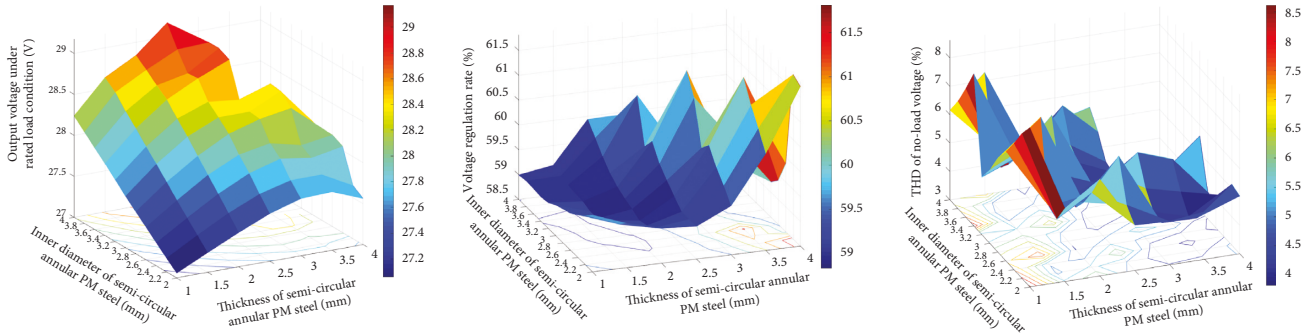

(a) (b) (c)

Figure 16: Variation diagrams of generator output performance with different thicknesses and inner diameters of semicircular annular PM steel: (a) output voltage under rated load condition; (b) voltage regulation rate; (c) THD of no-load voltage.

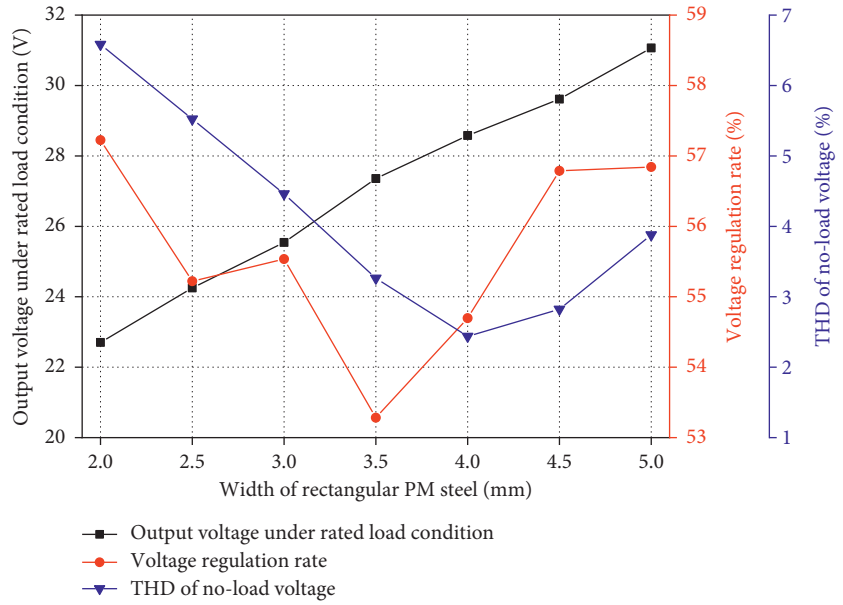

Figure 17: Variation curves of generator output performance with different widths of rectangular PM steel.

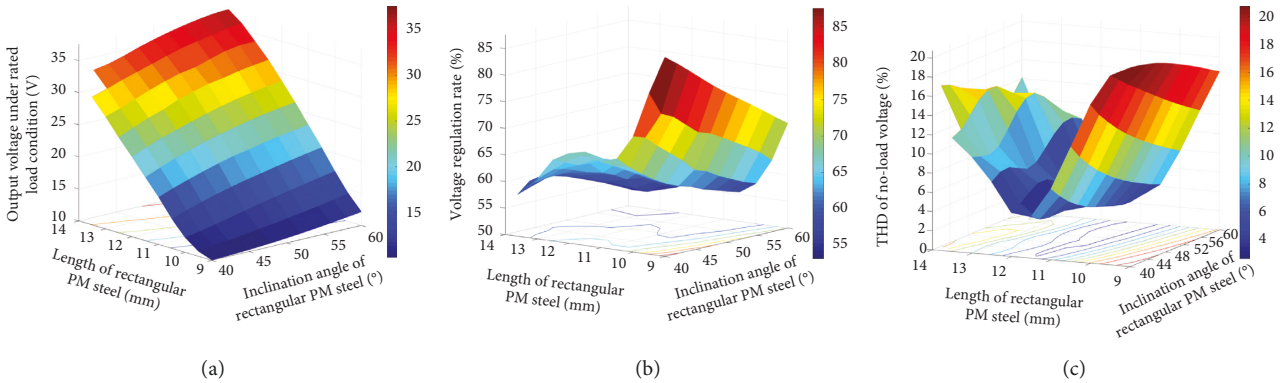

Figure 18: Variation diagrams of generator output performance with different inclination angles and lengths of rectangular PM steel: (a) output voltage under rated load condition; (b) voltage regulation rate; (c) THD of no-load voltage.

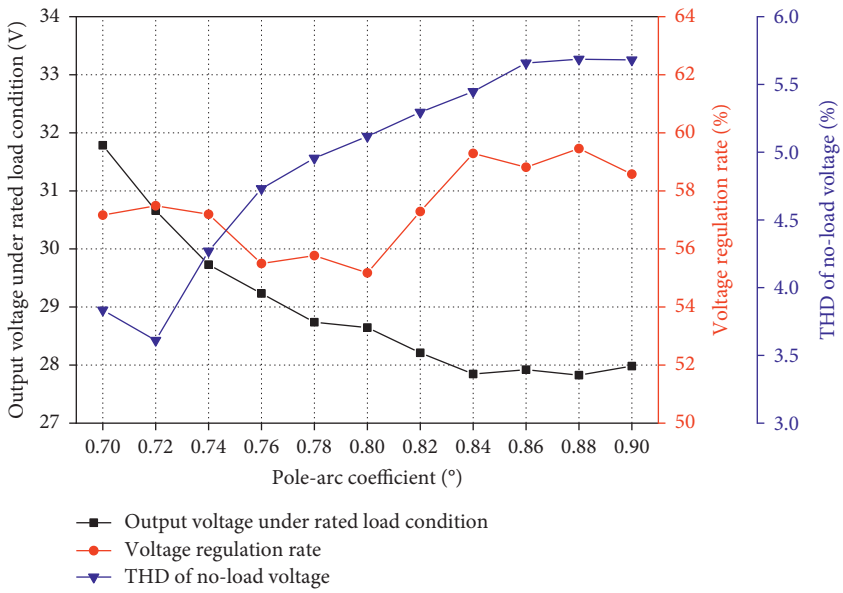

Figure 19: Variation curves of generator output performance with different pole-arc coefficients.

design of PM steel in the rotor pole shoe, when the pole-arc coefficient is low, the end of the rectangular PM steel will be close to the side of the rotor pole shoe, and the strength of the rotor structure will be reduced. Comprehensively considered, it is appropriate to select the pole-arc coefficient from 0.76 to 0.82.

According to the above analysis, the parameters of the generator armature reaction magnetic field are interrelated, so it is necessary to carry out the combined analysis of multiple parameters. In order to simplify the optimization analysis and reduce the number of combinations, the parameters with a clear change trend are selected to meet the optimized value of the rated output voltage, for example, the width and length of rectangular PM, the thickness of semicircular annular PM, etc. The parameters of combination optimization and their value ranges are shown in Table 3.

The 243 groups of parameter combinations of the 5 parameters in Table 2 are simulated and analyzed, and the variation curves of generator output voltage under rated load conditions, voltage regulation rate, and THD of no-load voltage with different groups are obtained, as shown in Figure 20 and Figure 21, respectively.

Figures 20 and 21 show that the rated load output voltage of the generator changes in a regular broken line shape, the voltage regulation rate changes in a regular broken line shape with three sections, and the average value is about 57.5%. The THD of no-load voltage decreases in a broken line shape, and the average value is about 4.5%.

According to the performance requirements of the generator, and based on the screening conditions that the generator output voltage is greater than 28 V, the voltage regulation rate is less than 57.5%, the THD of no-load voltage is less than 4.5%, and the inner diameter of semicircular annular PM steel is less than 2.7 mm; 17 groups are selected. In these 17 groups, the optimal outer length of the semicircular annular PM steel is 1 mm, the optimal inner diameter of the semicircular annular PM steel is 2.7 mm, the rotor eccentricities are 14 mm, 15 mm, and 16 mm, the pole-arc coefficients are 0.78, 0.8, and 0.82, and the inclination angles of rectangular PM steel are 54, 55, and 56. Since the designed generator is the HEG, it needs to analyze the influence of EEMF. Therefore, the excitation current is fixed at 2 A, the rated load power of HEG is 1000 W, and the variation curves of HEG output performance with different optimized groups are analyzed, as shown in Figure 22 and Figure 23, respectively.

Figures 22 and23 show that the voltage regulation rate of HEG is higher than that of a pure PM generator. Meanwhile, the combined parameters of rotor eccentricity and pole-arc coefficient are the main influencing parameters. Comparing the generator output voltage, voltage regulation rate, and THD of no-load voltage, group 6 is the best. In this case, the output voltage of HEG is 28.8 V, the voltage distortion rate is 57.43%, and the THD of no-load voltage is 4.42%. The optimized parameter values are shown in Table 4.

Table 3: Optimization parameters and their value range.

Optimization parameters	Value range
Rotor eccentricity	14 mm~16 mm
Outer length of semicircular annular PM steel	1 mm~1.2 mm
The inner diameter of semicircular annular PM steel	2.6 mm~2.8 mm
The inclination angle of rectangular PM steel	54~56
Pole-arc coefficient	0.76~0.82

4.1. Prototype Test and Performance Analysis of HEG. The prototype is trial manufactured and tested with the optimized parameters. The prototype structure and test bench are shown in Figure 24.

The no-load operation test of the HEG is carried out, and the no-load voltage waveform of the generator is obtained and compared with the simulation results, as shown in Figure 25.

Figure 25 shows that the no-load voltage waveform obtained by the performance test is basically the same as the simulation results, and the sinusoidality at the peak is lower than the simulation result. The no-load voltage waveform of the generator has good sinusoidality, and the sinusoidal distortion rate is 4.42%. The relationship curves between the generator output voltage and the speeds r_s with different excitation currents, also called the no-load characteristic curve of the generator, are analyzed and shown in Figure 26.

Figure 26 shows that with the increase of the generator speed, the output voltage increases linearly. When the excitation current is 0 A, it is the no-load characteristic curve of the HEG in the state of pure PM excitation, and it is almost a straight line. With the increase of excitation current, the inclination angle of the no-load characteristic curve increases, and the increased amplitude decreases. When the generator speed is from 400 r/min to 4000 r/min with an interval of 600 r/min, the variation curves of generator output voltage and excitation current are shown in Figure 27.

Figure 27 shows that at the same speed, with the increase of excitation current, the output voltage of the generator increases, and the trend is more obvious. Meanwhile, the increasing trend when the excitation current is less than 0 A is significantly greater than that when the excitation current is greater than 0 A. The reason is that the HEG is dominated by PM magnetic field and supplemented by EEMF, and the intensity of EEMF is less than that of the PM magnetic field. Therefore, with the increase of excitation current, the magnetic fields of the rotor and stator gradually tend to be saturated, the change of magnetic field becomes smaller, and the growth trend of output voltage also becomes smaller. When the generator operates at the rated speed, changing the size and direction of the excitation current to make the generator output the rated voltage under different load conditions, the relationship curve between the load current and the excitation current can be obtained. This curve is also called the HEG regulation characteristic curve, as shown in Figure 28.

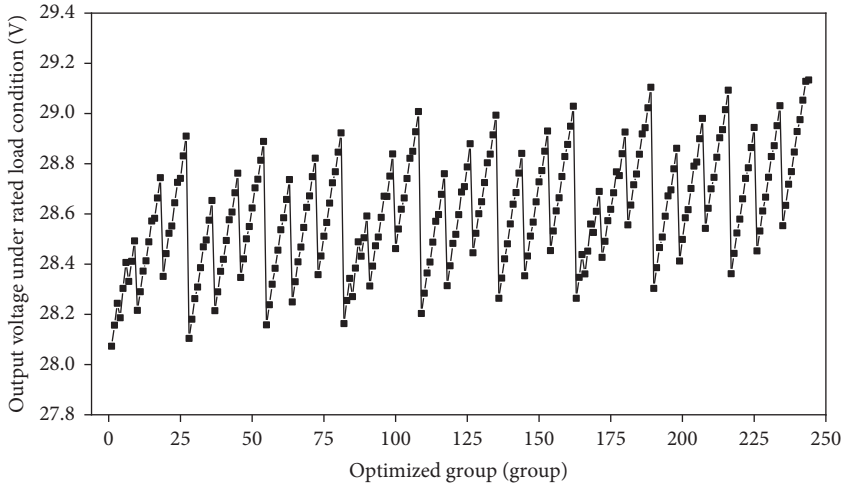

Figure 20: Variation curve of generator output voltage under rated load condition with different optimal groups.

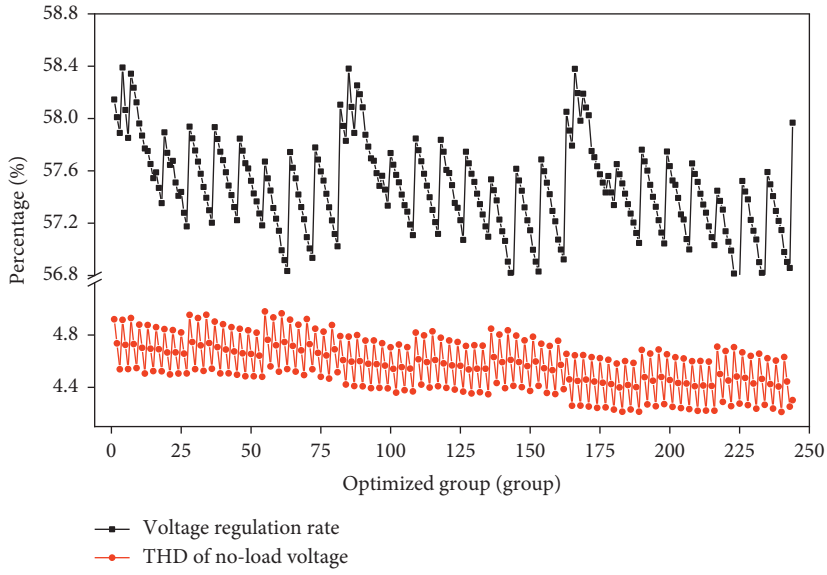

Figure 21: Variation diagrams of generator voltage regulation rate and THD of no-load voltage with different optimal groups.

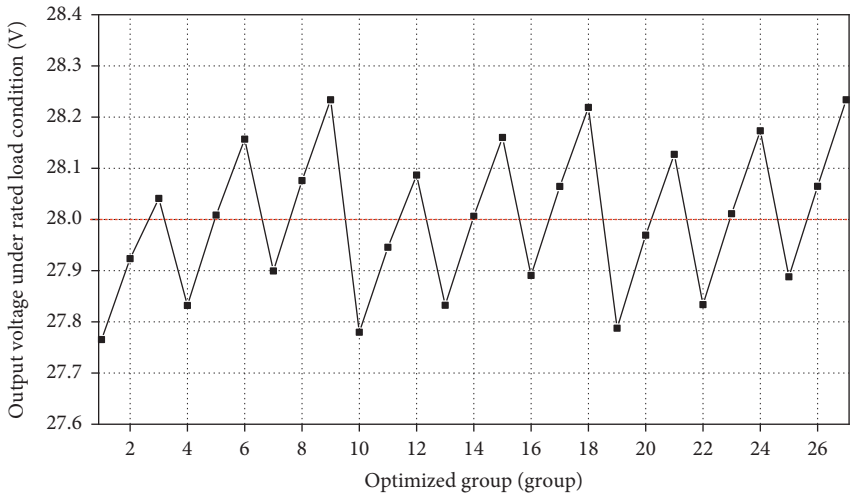

Figure 22: Variation curves of HEG output voltage under rated load conditions with different optimized groups.

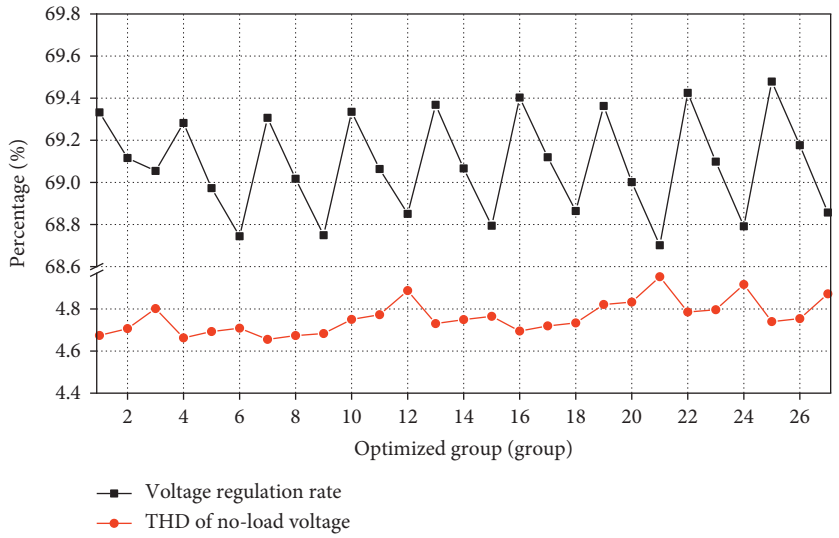

Figure 23: Variation diagrams of HEG voltage regulation rate and no-load voltage waveform distortion rate with different optimized groups.

Table 4: Optimization parameters and their value range.

Parameter	Parameter value	Parameter	Parameter value
Turns of armature winding	6 mm	Main air gap	0.4 mm
Width of stator notch	2.6 mm	Rotor eccentricity	15 mm
Width of stator slot	6.2 mm	Pole-arc coefficient	0.82
Outer length of semicircular annular PM steel	1 mm	Width of rectangular PM steel	4 mm
The thickness of semicircular annular PM steel	2 mm	Length of rectangular PM steel	12 mm
The inner diameter of semicircular annular PM steel	2.7 mm	The inclination angle of rectangular PM steel	56

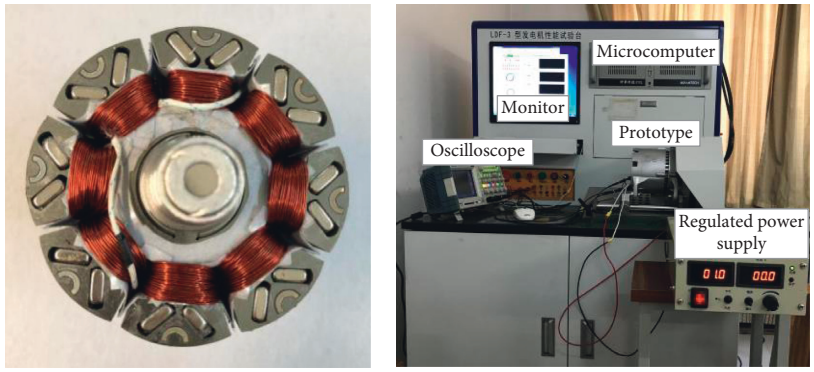

(a) (b)

Figure 24: Prototype of designed HEG and test bench: (a) rotor; (b) test bench.

Figure 28 shows that with the increase of load current, the load power of the generator increases, and the excitation current required to ensure the rated output voltage increases almost linearly. When the load current is greater than 32.1 A and the load power is greater than 900 W, the excitation current of the HEG needs to be greater than 0 A to ensure the rated output voltage. Meanwhile, the inclination of the regulation characteristic curve increases. In other words, increasing the same load current requires increasing more excitation current. On the contrary, when the load current is less than 28.6 A and the load power is less than 800 W, the excitation current needs to be less than 0 A to ensure the regulated output. Meanwhile, the inclination of the regulation characteristic curve is low, which shows that adjusting the excitation current can quickly change the output voltage. When the generator is under the rated load condition, the load power is 1000 W, and the load current is 35.7 A, the excitation current is only 1.8 A. In this case, the HEG is dominated by PM magnetic field and supplemented by EEMF to reduce the excitation loss. When the generator is in half load condition, the load power is 500 W, and the load current is 18 A, the excitation current is −3.6 A. In this case,

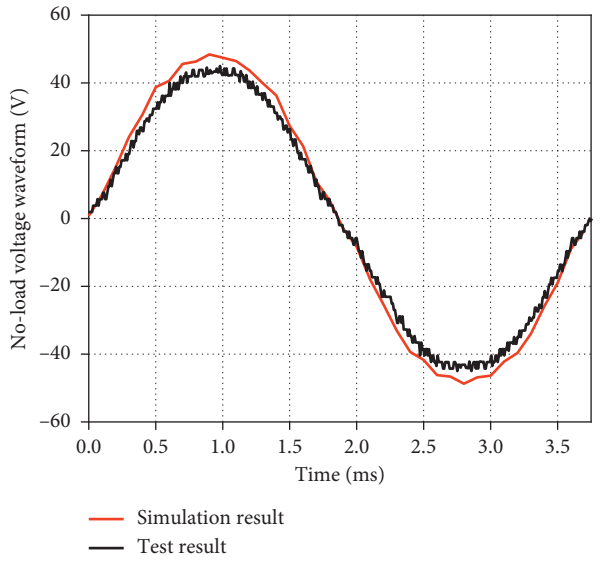

Figure 25: Comparison between test results and simulation results of the no-load voltage waveform of HEG.

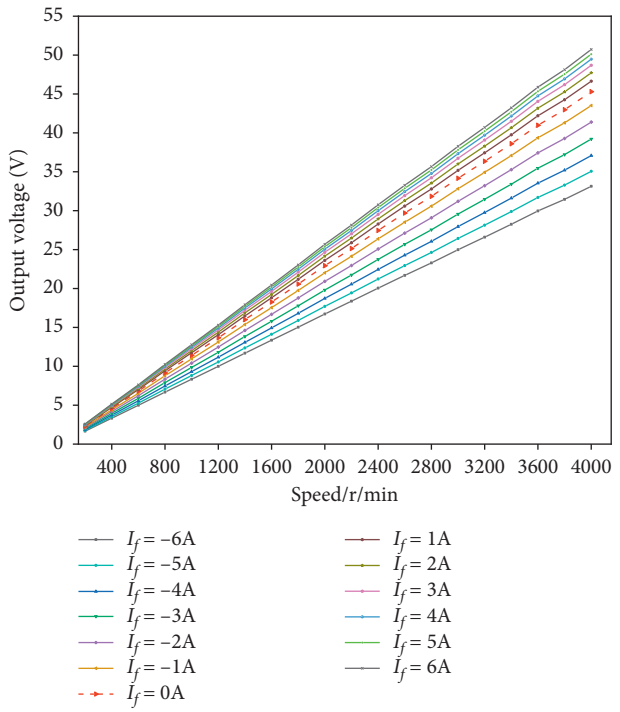

Figure 26: The no-load characteristic curve of HEG.

the EEMF weakens the PM magnetic field to achieve the purpose of stable output voltage. When the load power is 1200 W, the generator is in an overload condition and the excitation current is 5.8 A. The EEMF plays the role of increasing the synthetic magnetic field. Through comprehensive analysis, the designed HEG has good voltage regulation performance.

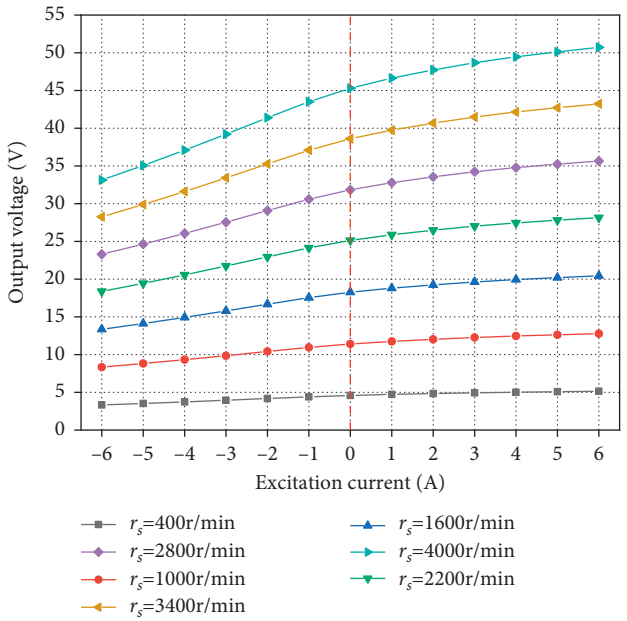

Figure 27: Variation curves of HEG output voltage and excitation current with different speeds.

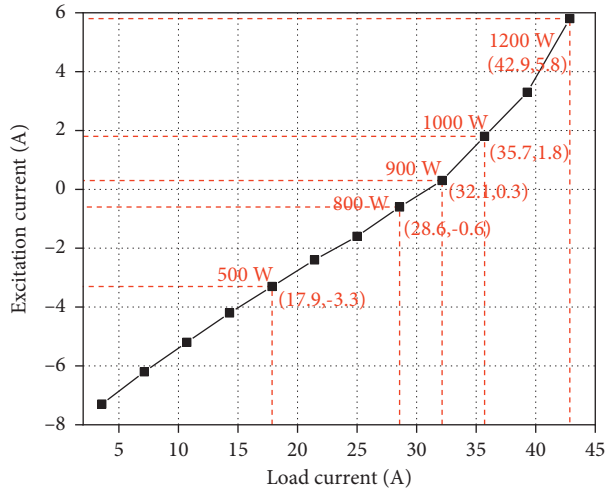

Figure 28: The regulation characteristic curve of the HEG.

5. Conclusions

This paper proposes a built-in PM and salient-pole electromagnetic HEG. The generator adopts the PM part as the main provider of output power, and the electric excitation part plays an auxiliary and regulating role. The HEG can reduce the complex voltage stabilizing circuit and expensive control components of pure PM generators and have the advantages of high power density and good regulation performance. The analytical expression of the armature reaction magnetic field of the HEG and its influencing factors are analyzed. Taking the generator output voltage

under rated load condition, voltage regulation rate, and THD of no-load voltage as the target, the influence of each parameter on the generator output performance is studied and analyzed to complete the parameter optimization. After optimization, the voltage regulation rate of HEG is 57.43%, and the THD of no-load voltage is 4.42%. The prototype is trial manufactured and tested, the results show that the HEG has good no-load characteristics and good regulating characteristics, and the designed generator can meet the application requirements.

Data Availability

All data used to support the findings of this study are available from the corresponding author upon request.

Conflicts of Interest

The authors declare that there are no conflicts of interest regarding the publication of this paper.

Acknowledgments

This research work was partially supported by the National Natural Science Foundation of China (Grant nos. 51875327 and 51975340).

References

[1] X. Gu, Z. Zhang, L. Sun, and L. Yu, "Magnetic field enhancement characteristic of an axially parallel hybrid excitation DC generator," *IEEE Transactions on Magnetics*, vol. 57, no. 2, pp. 1–5, 2021.

[2] J. Liu, Q. Zhang, R. Wang, J. Hu, L. Zhang, and B. Cai, "An asymmetric-primary Axis-flux hybrid-excitation generator for the vertical Axis wind turbine," *IEEE Access*, vol. 9, pp. 92318–92325, 2021.

[3] W. Sriwannarat, P. Seangwong, A. Sriwannarat, and P. Khunkitti, "An improvement of output power in doubly salient permanent magnet generator using Pole configuration adjustment," *Energies*, vol. 13, no. 17, pp. 1–14, 2020.

[4] A. Blanc, "Exciting field and quadrature-axis armature reaction in a cascade equivalent A-H-circuit of a salient-pole generator," *International Journal of Electrical and Computer Engineering*, vol. 10, no. 2, pp. 1674–1681, 2020.

[5] L. Sun, Z. Zhang, X. Gu, and L. Yu, "Analysis of a hybrid excitation brushless DC generator with an integrated shared-flux-path exciter," *IEEE Transactions on Industrial Electronics*, vol. 68, no. 8, pp. 6672–6681, 2021.

[6] J. Jiang, X. Zhang, X. Zhao, and S. Niu, "A novel winding switching control strategy for AC/DC hybrid-excited wind power generator," *IEEE Transactions on Magnetics*, vol. 57, no. 6, pp. 1–4, 2021.

[7] E. Ilhan, M. F. J. Kremers, T. E. Motoasca, J. J. H. Paulides, and E. A. Lomonova, "Nonlinear performance characteristics of flux-switching PM motors," *Journal of Engineering*, vol. 2013, Article ID 593434, 8 pages, 2013.

[8] X. Zhang, Q. Du, J. Xu, and Y. Zhao, "Development and analysis of the magnetic circuit on double-radial permanent magnet and salient-Pole electromagnetic hybrid excitation generator for vehicles," *Chinese Journal of Mechanical Engineering*, vol. 32, no. 2, pp. 100–112, 2019.

[9] A. Padilla-Garcia, G. Gonzalez-Avalos, N. Barrera-Gallegos, and G. Ayala-Jaimes, "A quasi-steady state model of a singularly perturbed wind turbine with an induction generator and nonlinear frictions: a bond graph approach," *Journal of Engineering*, vol. 2020, pp. 1–26, 2020.

[10] M. Julius, L. Hui, and Z. Dai, "A condensed introduction to the doubly fed induction generator wind energy conversion systems," *Journal of Engineering*, vol. 2017, Article ID 2918281, 18 pages, 2017.

[11] J. Hou, W. Geng, Q. Li, and Z. Zhang, "3-D equivalent magnetic network modeling and FEA verification of a novel axial-flux hybrid-excitation in-wheel motor," *IEEE Transactions on Magnetics*, vol. 57, no. 7, pp. 1–12, 2021.

[12] M. Julius, L. Hui, and Z. Dai, "A concise presentation of doubly fed induction generator wind energy conversion systems challenges and solutions," *Journal of Engineering*, vol. 2017, Article ID 4015102, 13 pages, 2017.

[13] H. Geng, X. Zhang, L. Tong et al., "Performance optimization analysis of hybrid excitation generator with the electromagnetic rotor and embedded permanent magnet rotor for vehicle," *IEEE Access*, vol. 9, pp. 163640–163653, 2021.

[14] Z. Xing, S. Niu, and X. Zhang, "Design of a new relieving-DC-saturation hybrid excitation vernier machine for HEV starter generator application," *IEEE Transactions on Industrial Electronics*, vol. 67, no. 8, pp. 6342–6353, 2020.

[15] Z. Xing, S. Niu, and W. Fu, "Sensitivity analysis and design optimization of a new hybrid-excited dual-PM generator with relieving-DC-saturation structure for stand-alone wind power generation," *IEEE Transactions on Magnetics*, vol. 56, no. 1, pp. 1–5, 2020.

[16] H. Geng, X. Zhang, Y. Zhang et al., "Development of brushless claw Pole electrical excitation and combined permanent magnet hybrid excitation generator for vehicles," *Energies*, vol. 13, no. 18, pp. 1–13, 2020.

[17] Q. Lu, B. Wu, Z. Zeng, and X. Huang, "Analysis of a new partitioned-primary flux-reversal hybrid-excited linear motor," *IEEE Transactions on Industry Applications*, vol. 57, no. 1, pp. 448–457, 2021.

[18] E. F. Farahani, M. A. J. Kondelaji, and M. Mirsalim, "An innovative hybrid-excited multi-tooth switched reluctance motor for torque enhancement," *IEEE Transactions on Industrial Electronics*, vol. 68, no. 2, pp. 982–992, 2021.

[19] T. Yang and Q. Cao, "Dynamics and energy generation of a hybrid energy harvester under colored noise excitations," *Mechanical Systems and Signal Processing*, vol. 121, pp. 745–766, 2019.

[20] S. Nuzzo, P. Bolognesi, G. Decuzzi, P. Giangrande, and M. Galea, "A consequent-Pole hybrid exciter for synchronous generators," *IEEE Transactions on Energy Conversion*, vol. 36, no. 1, pp. 368–379, 2021.

[21] L. Sun, Z. Zhang, Y. Li, and X. Gu, "Development and analysis of a new hybrid excitation brushless DC generator with flux modulation effect," *IEEE Transactions on Industrial Electronics*, vol. 66, no. 6, pp. 4189–4198, 2019.

[22] W. J. Hu, X. Y. Zhang, H. B. Yin, G. Huihuri, Z. Yufeng, and L. Shi, "Analysis of magnetic field and electromagnetic performance of a new hybrid excitation synchronous motor with dual-V type magnets," *Energies*, vol. 13, no. 6, pp. 1–19, 2020.

[23] E. Spooner, S. A. W. Khatab, and N. G. Nicolaou, "Hybrid excitation of AC and DC machines," in *Procedings of the Fourth International Conference On Electrical Machines And Drives*, pp. 48–52, London, UK, 1989.

[24] Y. Burkhardt, K. Schleicher, and M. Klöpzig, "A novel hybrid excited synchronous machine for (H)EV applications," in

Proceedings of the International Conference on Electrical Machines (ICEM), pp. 353–359, Berlin, Germany, 2014.

[25] J. A. Tapia, F. Leonardi, and T. A. Lipo, "Consequent-pole permanent-magnet machine with extended field-weakening capability," *IEEE Transactions on Industry Applications*, vol. 39, no. 6, pp. 1704–1709, 2003.

[26] W. Hu, X. Zhang, H. Geng, T. Gao, L. Shi, and D. You, "Electromagnetic design and flux regulation analysis of new hybrid excitation generator for electric vehicle range extender," *Journal of Electrical and Computer Engineering*, vol. 2021, no. 18, pp. 1–13, 2021.

[27] W. Li, S. Huang, and Q. Zhang, "Multi-domain simulation analysis of a hybrid excitation claw-pole belt-alternator starter generator for hybrid electrical vehicles," *Proceedings of the CSEE*, vol. 30, no. 36, pp. 7–15, 2010, (in Chinese).

[28] X. Zhang, Q. Du, S. Ma, W. Hu, and H. Geng, "Magnetic flux analysis and performance test of permanent magnet and claw-pole electromagnetic hybrid excitation generator for electric vehicle range extender," *International Journal of Electric and Hybrid Vehicles*, vol. 9, no. 3, pp. 187–205, 2017.

[29] S. Wang, Y. Xia, S. Huang, A. Qiu, and X. Wang, "Research on new hybrid excitation PM synchronous generators with tooth harmonic excitation," *COMPEL: The International Journal for Computation and Mathematics in Electrical and Electronic Engineering*, vol. 33, no. No. 5, pp. 1613–1624, 2014.

[30] J. T. Chen, Z. Q. Zhu, S. Iwasaki, and R. Deodhar, "A novel e-core flux-switching pm brushless ac machine," in *Proceedings of the IEEE Energy Conversion Congress and Exposition*, pp. 3811–3818, Atlanta, GA, USA, 2010.

[31] Q. Wang and S. Niu, "Design, modeling, and control of a novel hybrid-excited flux-bidirectional-modulated generator-based wind power generation system," *IEEE Transactions on Power Electronics*, vol. 33, no. 4, pp. 3086–3096, 2018.

[32] S. Zhu Shushu, C. Liu Chuang, Y. Ning Yinhang, and J. Tang Jie, "A two-stage brushless excitation method for hybrid excitation synchronous generator," *IEEE Transactions on Magnetics*, vol. 51, no. 6, pp. 1–11, 2015.

[33] S. Kusase and K. Kurihara, "New hybrid-excited motor using armature windings as field flux source," *Electrical Engineering in Japan*, vol. 202, no. 1, pp. 41–48, Jan. 2018.

[34] X. Zhang, Q. Du, S. Ma et al., "Permeance analysis and calculation of the double-radial rare-earth permanent magnet voltage-stabilizing generation device," *IEEE Access*, vol. 6, pp. 23939–23947, 2018.

[35] H. Wang, Z. Wu, K. Liu, and J. Wei, "Analysis and comparison of armature fields and inductances in various topologies of compulsators," *IEEE Transactions on Plasma Science*, vol. 48, no. 12, pp. 4228–4234, 2020.

[36] J. S. Jang, J. K. Lee, and B. T. Kim, "Characteristic analysis of a hybrid excited flux switching PM motor by using the equivalent magnetic circuit method," *International Journal of Applied Electromagnetics and Mechanics*, vol. 39, no. 1-4, pp. 843–849, 2012.